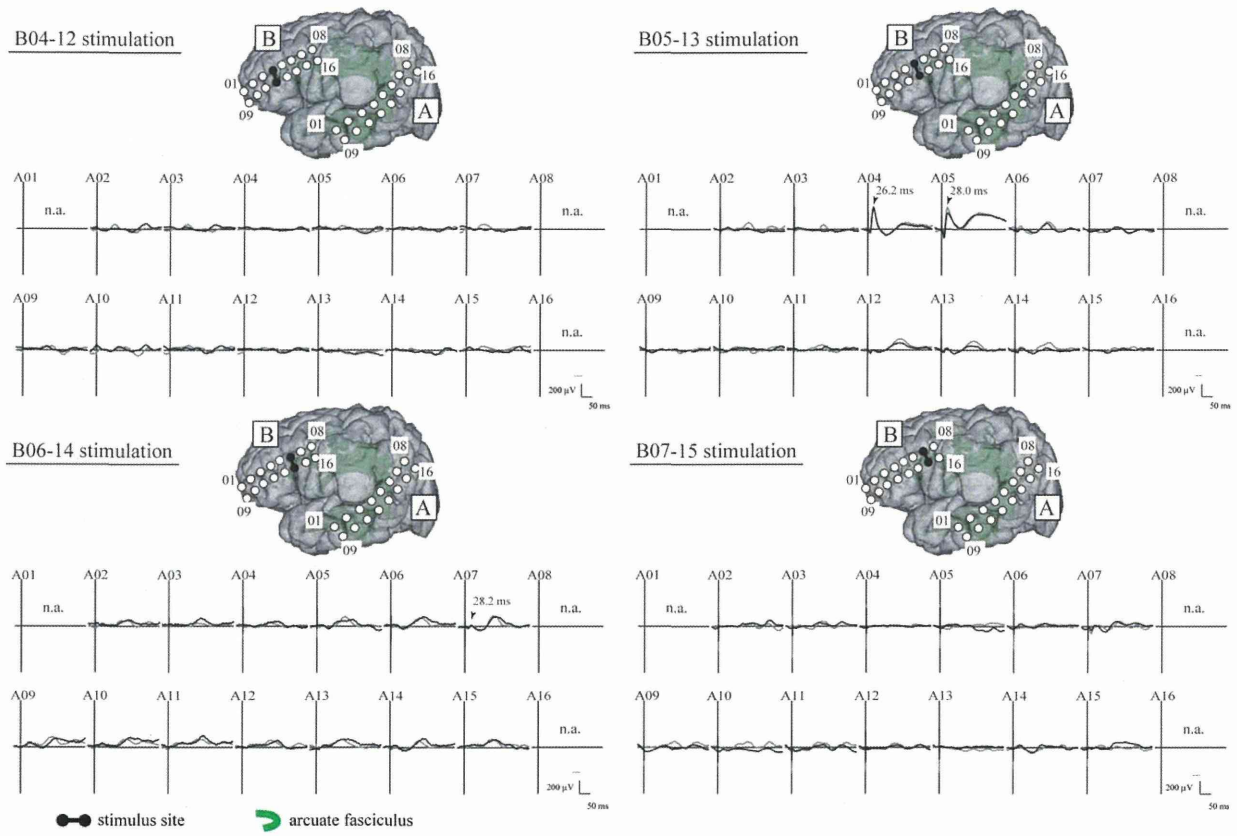

Figure 3.

CCEP connectivity pattern to map perisylvian language areas (Patient 4). Under general anesthesia, single-pulse ES was delivered to four candidate sites (Plate B) according to the noninvasive anatomo-functional mapping, and CCEPs were recorded from the temporoparietal area (Plate A). Two trials are plotted in superimposition at each electrode. The vertical bar corresponds to the time of stimulation. Note the CCEP pattern in Plate A differs evidently among the four stimulus sites. Electrode B05–13 stimulation showed the largest and most discrete CCEP response in the lateral temporoparietal area (Electrode A04 and A05). This site was regarded as the putative anterior language area. Indeed 50 Hz stimulation of this area showed language impairment in the awake condition. n.a. = CCEP was not available due to high impedance in the recording electrode. Other conventions are the same as for Figure 1.

changed by an average of 0.7 ms (ranging from −0.2 to 1.8).

Waveforms sequentially recorded from a representative case (Patient 3) are shown in Figure 4. The maximum CCEP response was recorded at Electrode B02 on the STG. In this electrode, the N1 amplitude changed from 215 to 311 μV when the patient awoke from general anesthesia. The amplitude did not decline after total removal of the tumor, and she did not have language dysfunction during or after surgery.

In all patients, online CCEP monitoring was sequentially performed in the awake condition. The N1 amplitude at the maximum CCEP response site was compared with that at the beginning of the awake condition (Fig. 2). In four of six patients, the N1 amplitude did not decrease after tumor resection. In Patient 2, the N1 amplitude decreased from 500 to 440 μV (−12%) after tumor resection. She did not show any language dysfunction during or after surgery. In Patient 4, the N1 amplitude changed from 383 to 260 μV (−32%) after tumor resection (Fig. 2). This patient showed phonemic paraphasia and dyscalculia immediately after waking up. This was most likely due to the partial resection of the left SMG cortex during general anesthesia. No further language deficits developed during tumor removal in the white matter despite the 32% decrease of the N1 amplitude. This patient showed a postoperative decline in the WAB aphasia quotient (80) but she had recovered fully 3 months after surgery (100). In Patient 5, the N1 amplitude of the maximum CCEP response site was 197 and 227 μV before and after tumor resection,

TABLE II. CCEP connectivity pattern

	Frontal stimulus sites (location of electrode pair)			$CCEP_{AL \rightarrow PL}$ response				Consistency with fMRI (language cortex)		Consistency with diffusion tractography (the AF tract)	
	IFGtr	IFGop	MFG	STG	MTG	ITG	AG/SMG	AL	PL	AL	PL
Patient 1	+			+		+	++	Yes	Yes	Yes	Yes
Patient 2	+	+		+	++		+	Yes	Yes	Yes	No
Patient 3	+	+		++	+	+		Yes	Yes	Yes	Yes
Patient 4	+			++	+			Yes	n.a.	Yes	Yes
Patient 5			+	++			+	Yes	n.a.	Yes	No
Patient 6	+	+		+	+	++		Yes	Yes	No	Yes

IFGtr = inferior frontal gyrus pars triangularis; IFGop = inferior frontal gyrus pars opecularis; MFG = middle frontal gyrus; STG = superior temporal gyrus; MTG = middle temporal gyrus; ITG = inferior temporal gyrus; AG = angular gyrus; SMG = supramarginal gyrus; AF = arcuate fasciculus; AL = anterior language area; PL = posterior language area; n.a. = not available (no fMRI activation); ++ the largest CCEP response

TABLE III. Intraoperative language network mapping and functional outcome

	Cortical HFES at the frontal stimulus site	$CCEP_{AL \rightarrow PL}$ N1 latency (ms)		CCEP amplitude decrease (%)	Subcortical HFES at WM stimulus site	SCEP N1 latency (ms)					Language disturbance	
						$SCEP_{WM \rightarrow AL}$		$SCEP_{WM \rightarrow PL}$		$SCEP_{WM \rightarrow AL} + SCEP_{WM \rightarrow PL}$		
	Language impairment	Onset	Peak		Language impairment	Onset	Peak	Onset	Peak	Onset/ peak	Intraoperative	Postoperative (day 1)
Patient 1	Yes	7.6	30.8	0	No	no response		no response		no response	No	No
Patient 2	Yes	12.8	27.4	12	n.a.	n.a.	n.a.	n.a.	n.a.	n.a.	No	No
Patient 3	Yes	12.8	29.2	0	Yes	5.6	24.6	6.4	19.6	12.0/44.2	No	No
Patient 4	Yes	11.0	25.0	32	Yes	7.2	19.0	4.2	12.0	11.4/31.0	Yes[a]	Yes
Patient 5	Yes	9.6	32.0	0	Yes	6.2	17.6	4.0	15.8	10.2/33.4	No	Yes
Patient 6	Yes	13.0	33.2	0	No	6.6	22.6	3.2	18.0	9.8/40.6	No	No

All latencies were measured in the awake condition.
HFES = high-frequency electrical stimulation; AL = anterior language area; PL = posterior language area; WM = white matter; n.a. = not available (no stimulation).
[a]Language disturbance was already observed before the CCEP amplitude decreased because of the partial cortical resection of the supramarginal gyrus

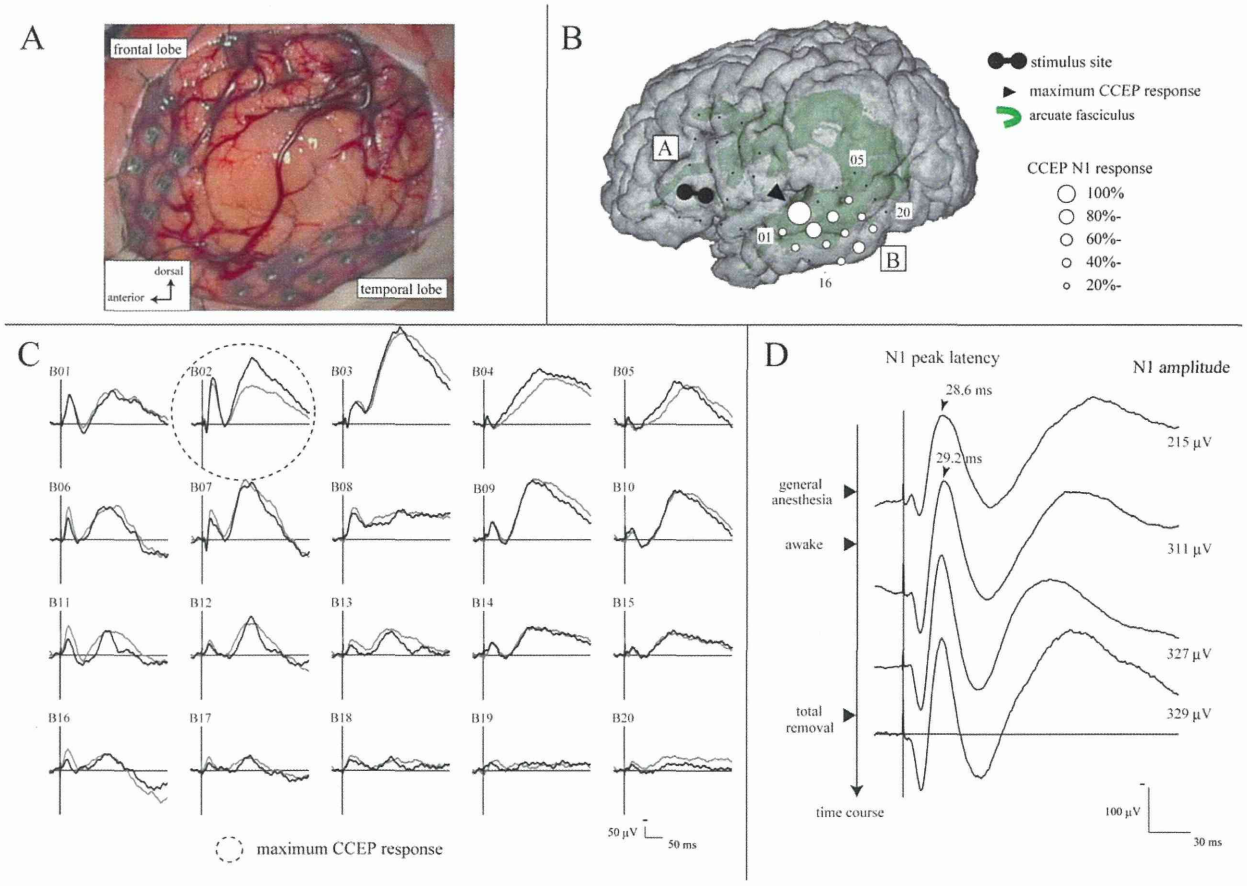

Figure 4.

Intraoperative online language network mapping by CCEPs (Patient 3). **A**: Electrode configuration in the intraoperative view. **B**: CCEP distribution map during general anesthesia. CCEP distributed over the middle to posterior part of the superior, middle and inferior temporal gyri (the maximum at Electrode B02 in the superior temporal gyrus). **C**: CCEP waveforms (Plate B) in the awake condition (before tumor removal). Two trials are plotted in superimposition. CCEP distribution did not change between general anesthesia and awake condition. **D**: Change of the N1 amplitude during surgery at the maximum CCEP response site (Electrode B02). CCEP waveforms are sequentially shown from the top to the bottom along the time course of surgery. As the patient awoke, the N1 amplitude increased from 215 to 311 μV (+45%). After tumor removal the N1 amplitude did not decline (329 μV). She did not show language dysfunction during or after surgery. Other conventions are the same as for Figure 3.

respectively (Fig. 2). The N1 amplitude itself did not decline and he did not show any language dysfunction during surgery. The patient, however, developed a decline in verbal fluency, detected by routine neurological examination, immediately after surgery. This temporary symptom might have been caused by postoperative brain edema as judged from MRI findings, and he had recovered fully 2 months after surgery.

In summary, during tumor resection in the awake condition, CCEP amplitude decreased by 12 or 32% in two patients (Patients 2 and 4). One patient (Patient 4) developed intraoperative language impairment, most likely due to cortical resection, and another patient (Patient 5) developed language impairment immediately after surgery because of brain edema. Language function recovered within a few months in both patients, and none of them had persistent language impairment.

The results of intraoperative monitoring and functional outcome are summarized in Table III and partly in Table I (WAB scores).

Intraoperative Subcortical Stimulation

In four of five patients, white matter stimulation (1 Hz) elicited SCEP both at the ventrolateral frontal area (the putative AL) and temporoparietal area (the putative PL) successfully. The results are summarized in Table IV.

Frontal SCEP responses were recorded in the IFGtr in three patients, the IFGop in three, IFGor in three, and the most caudal part of the MFG in three. In all four patients, the frontal stimulus site for CCEPs was located within the frontal SCEP response sites. The location of the frontal SCEP response site was consistent with that of fMRI activation in all patients and the cortical terminations of the AF tract in three.

Upon stimulation of the white matter, SCEPs were recorded from the STG in four patients, MTG in four, ITG in two, and AG/SMG in one. In all four patients, the temporoparietal site of the maximum CCEP response was located within the temporoparietal SCEP response sites. The distribution of SCEP response sites was consistent with fMRI activation in two patients, and the cortical terminations of the AF tract in two.

In three of five patients (Patients 3–5), high-frequency ES of the white matter produced language impairment in the picture naming task. Arrest of naming was elicited in Patients 3 and 4, and slower naming in Patient 5. The results of white matter functional mapping were consistent with the postoperative tractography study (Supporting Information Fig. 1). Stimulus sites at the floor of removal cavity were close to the AF tract (<6 mm) in three patients (Patients 3–5) who showed naming impairment, while the stimulus site was distant from the AF tract in Patients 1 and 6, who did not.

Waveforms obtained from a representative case (Patient 3) are shown in Figure 5. Circle maps are based on the SCEP amplitude percentage distribution. The largest amplitude SCEP at the putative AL ($SCEP_{WM\rightarrow AL}$) was recorded at Electrode B07 on the IFGtr and that at the putative PL ($SCEP_{WM\rightarrow PL}$) was recorded at Electrode A12 on the MTG. Electrode B07 corresponded with the stimulus site for CCEPs. At Electrode B07, the N1 onset latency of $SCEP_{WM\rightarrow AL}$ was 5.6 ms and the N1 peak latency was 24.6 ms. At Electrode A12, the N1 onset latency of $SCEP_{WM\rightarrow PL}$ was 6.4 ms and the peak latency was 19.6 ms. When the latencies of these two SCEPs, namely, $SCEP_{WM\rightarrow AL}$ and $SCEP_{WM\rightarrow PL}$, were compared with that of $CCEP_{AL\rightarrow PL}$, the sum of SCEP N1 onset latencies (5.6 ms + 6.4 ms = 12.0 ms) approximately corresponded with the onset latency of $CCEP_{AL\rightarrow PL}$ (12.8 ms). The sum of the SCEP N1 peak latencies (44.2 ms) was larger than that of $CCEP_{AL\rightarrow PL}$ (29.2 ms). A similar tendency ($SCEP_{WM\rightarrow AL} + SCEP_{WM\rightarrow PL} \approx CCEP_{AL\rightarrow PL}$) was observed for the onset latencies in Patients 4 and 5, but not in Patient 6 [9.8 ms (sum of SCEPs) vs. 13.0 ms ($CCEP_{AL\rightarrow PL}$)]. In Patient 6, considering that the stimulus site was distant from the AF, evoked potentials elicited by single-pulse ES likely represented cortico-cortical responses from the cortex in the removal cavity.

TABLE IV. SCEP connectivity pattern

	$SCEP_{WM\rightarrow AL}$ response				$SCEP_{WM\rightarrow PL}$ response				Consistency with fMRI (language cortex)		Consistency with diffusion tractography (the AF tract)	
	IFGor	IFGtr	IFGop	MFG	STG	MTG	ITG	AG/SMG	AL	PL	AL	PL
Patient 3	+	+	++	+	+	+	++		Yes	Yes	Yes	Yes
Patient 4	+	++	+	+	+	++			Yes	n.a.	Yes	Yes
Patient 5				++	+	++		+	Yes	n.a.	Yes	No
Patient 6	+	+	++		++	+	+		Yes	Yes	No	No

Only patients in whom SCEP was recorded successfully are shown.
IFGtr = inferior frontal gyrus pars orbitalis; IFGtr = inferior frontal gyrus pars triangularis; IFGop = inferior frontal gyrus pars opecularis; MFG = middle frontal gyrus; STG = superior temporal gyrus; MTG = middle temporal gyrus; ITG = inferior temporal gyrus; AG = angular gyrus; SMG = supramarginal gyrus; AF = arcuate fasciculus; AL = anterior language area; PL = posterior language area; WM = white matter; n.a. = not available (no fMRI activation); ++ the largest SCEP response

DISCUSSION

By applying 50 Hz and single-pulse ES to patients undergoing awake surgery for brain tumors around the AF, we demonstrated that (1) the CCEP connectivity pattern, when combined with preoperative neuroimaging studies, was able to map the AL and PL, (2) combined (50

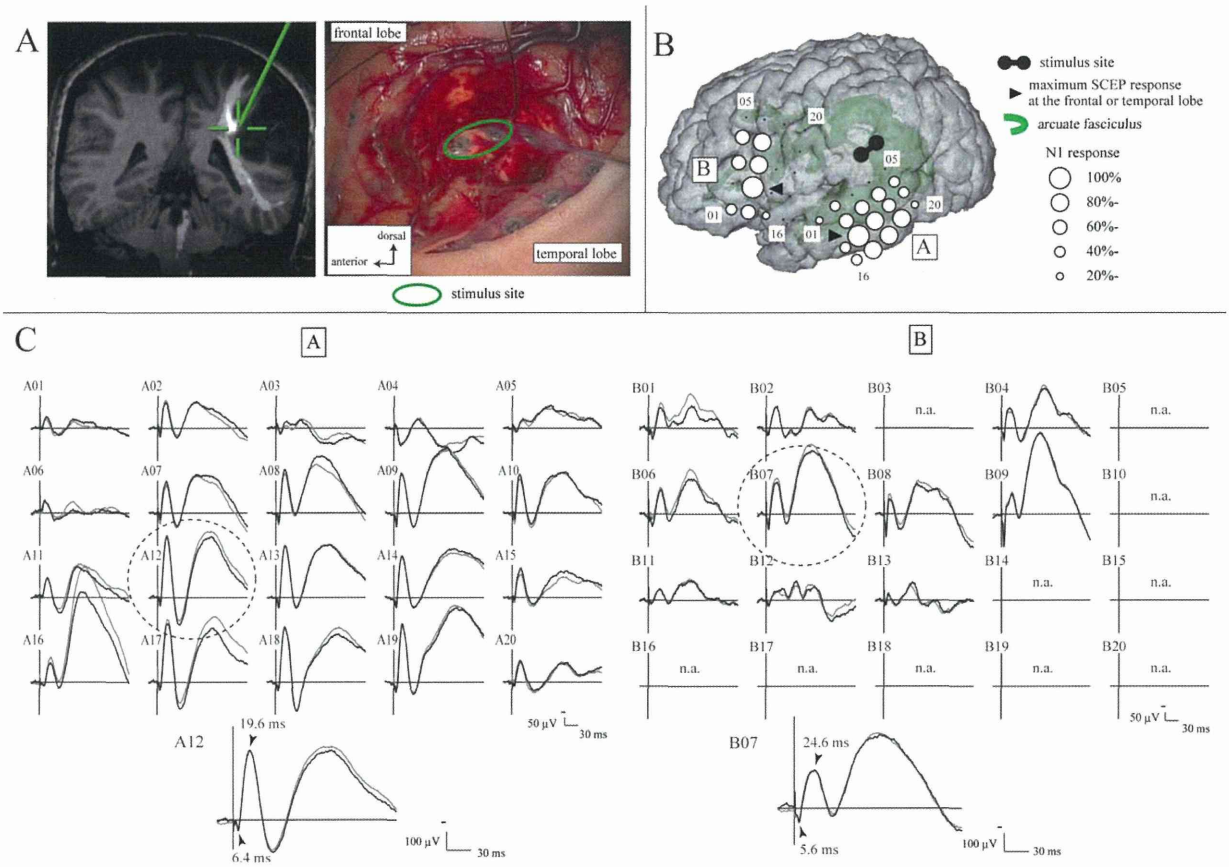

Figure 5.

SCEPs in Patient 3. **A**: Site of white matter stimulation. Electrode pair (highlighted by a green circle) was stimulated at the floor of the removal cavity (right). The stimulus site (cross hairs) was attached to the AF (long segment) in the neuro-navigation (left). High-frequency (50 Hz) stimulation at this site induced the arrest of naming. **B**: SCEP distribution in the frontal and temporal areas. Circle maps were made separately for SCEP responses in the frontal ($SCEP_{WM \rightarrow AL}$) and temporal ($SCEP_{WM \rightarrow PL}$) areas, based on the SCEP amplitude percentage distribution. **C**: $SCEP_{WM \rightarrow AL}$ (Plate B) and $SCEP_{WM \rightarrow PL}$ (Plate A) waveforms. The largest response was highlighted with a dotted circle and its onset and peak latencies are shown in the enlarged waveform at the bottom. n.a. = SCEP was not available due to the limited number of channels available for simultaneous monitoring or high impedance in the recording electrode. Other conventions are the same as for Figure 4.

Hz and single-pulse) white matter ES delineated both the function and cortical terminations of the "eloquent" language fibers, and (3) intraoperative online CCEP monitoring successfully prevented persistent language impairment in our case series. To the best of our knowledge, we proposed, for the first time, the intraoperative language network monitoring method by employing ES for functional mapping (50 Hz) and tract-tracing (1 Hz).

Subcortical Pathway of the Dorsal Language Network

Hickok and Poepple proposed a dual stream model for language processing [Hickok and Poeppel, 2004]. The dorsal stream engages in auditory-motor integration by mapping acoustic speech sounds to the articulatory representations, while the ventral stream serves as a sound-to-meaning interface. Recent diffusion tractography studies have revealed that the AF is divided into three components: the anterior, posterior, and long segments. The long segment of the AF connects the IFGop, IFGtr, MFG, and the precentral gyrus to the STG, MTG and ITG, and courses through the parietal lobe without sending projections to the parietal cortex [Catani et al., 2012; Glasser and Rilling, 2008]. The trajectory of the long segment was recently confirmed by a study combining diffusion tractography and postmortem fiber dissection [Martino et al., 2013].

To probe the function of the "language" fibers such as the long segment of the AF, high-frequency ES has been

applied to a part of the white matter tract and induced phonemic paraphasia [Kamada et al., 2007; Leclercq et al., 2010]. Even with this gold standard method, we could only obtain evidence that the white matter tract at the stimulus site, i.e., that "one spot" is involved in phonemic processing. We cannot fully argue that this "eloquent spot" constitutes a part of the dorsal language stream.

By applying single-pulse ES to a part of the cortices and by recording CCEPs from the remote cortical regions, we have delineated cortico-cortical networks involved in seizure propagation, as well as various cortical functions, in the extraoperative setting [Enatsu et al., 2013; Matsumoto et al., 2004, 2005, 2007, 2012]. By defining the language cortices using 50 Hz ES, we have demonstrated that the AL and PL are functionally connected with each other [Matsumoto et al., 2004]. In the present intraoperative study, we employed white matter 50 Hz and single-pulse ES in an attempt to obtain evidence that the "eloquent spot" connects to both the AL and PL, thereby constituting a part of the eloquent language pathways. In three patients (Patients 3–5), we were able to functionally map the "eloquent spot" at or close to the AF (within 6 mm) by 50 Hz ES. By recording SCEPs, single-pulse ES successfully traced the connections from the stimulus site, i.e., the eloquent spot, into the AL and PL as defined by noninvasive (fMRI, tractography) and invasive (50 Hz ES) findings. In summary, the present combined cortical- and subcortical ES study provided the direct evidence, for the first time, that the AL, PL, and AF (long segment) constitute the dorsal language network. The present findings support a previous noninvasive study in healthy subjects that traced the AF tract between the frontal and temporal areas activated during sublexical repetition of speech to propose the existence of a dorsal language route for sensorimotor mapping of sound to articulation [Saur et al., 2008]. We failed to produce phonemic paraphasia during white matter high-frequency ES probably because we used relatively high intensity of electric current (10–15 mA). Stimulation at higher intensity in this pilot study as compared with previous studies [Duffau et al., 2005; Kamada et al., 2007; Maldonado et al., 2011] likely resulted in the arrest or slowing of naming. High-frequency white matter ES at a lower intensity may be warranted for functional characterization of the dorsal language pathway in future investigations.

Implication of CCEP and SCEP

In extraoperative settings, CCEP has been extensively employed to investigate functional cortical networks and seizure propagation tracts [Catenoix et al., 2005, 2011; Keller et al., 2011; Koubeissi et al., 2012; Kubota et al., 2013; Lacruz et al., 2007; Matsumoto et al., 2004; Matsuzaki et al., 2013; Rosenberg et al., 2009]. It has been effective in locating inter-connected cortical regions, but its precise generator mechanism still remains unclear. Two possible modes of impulse propagation have been proposed: direct cortico-cortical propagation through white matter tracts, and indirect cortico-subcortico-cortical propagation via subcortical structures. Our recent parietofrontal connectivity study showed a linear correlation between the N1 peak latency and the surface distance from the parietal stimulus site to the frontal response site [Matsumoto et al., 2012]. This observation favors the direct cortico-cortical white matter pathway, because the longer the surface distance is, the proportionally longer the actual white matter pathway connecting the two cortical sites and, accordingly, its traveling time, is. Indeed, short latency CCEPs were recorded from the parietal depth electrodes in the superior longitudinal fasciculus by single pulse ES of the premotor area in another study [Enatsu et al., 2013]. In the present study, a comparison between SCEP and CCEP latencies provided further insight into the mode of impulse propagation. In three patients (Patients 3–5) in whom we successfully traced the connections from the AF to the cortical language areas by SCEPs, it was the sum of SCEP N1 onset latencies that approximately corresponded with the onset latency of $CCEP_{AL \rightarrow PL}$. The N1 onset or the first positive deflection is proposed to represent the fastest monosynaptic impulse projecting into the middle or deep cortical layers via large cortico-cortical projection fibers, giving rise to a small positive surface potential [Felleman and Van Essen, 1991; Terada et al., 2012]. If this is the case, our findings support the hypothesis that the impulse is conveyed directly through the white matter pathways. On the other hand, the sum of the SCEP N1 peak latencies was longer than $CCEP_{AL \rightarrow PL}$ N1 peak latency. The CCEP N1 peak likely represents the summation of direct cortico-cortical impulses conveyed both by small fibers with slower conduction velocities and by large myelinated fibers activated through indirect oligo-synaptic cortico-cortical projections. In this sense, as in intraoperative MEP monitoring, it is plausible to use the N1 amplitude as a surrogate marker of the integrity of the white matter tract.

Clinical Relevance of Intraoperative Language Network Monitoring

Under general anesthesia, single-pulse ES was applied to several candidate cortical locations for the frontal stimulus site (the putative AL) according to the noninvasive anatomical (gyral patterns) and functional (fMRI) findings. By comparing CCEP distribution with the anatomy (terminations of the AF tract) and function (fMRI) in the lateral temporoparietal area, the frontal stimulus site, namely, the putative AL, was determined in each patient. Of note, the CCEP connectivity pattern successfully localized the frontal stimulus site at the core AL where high-frequency ES produced language impairment in all patients. Functional cortical mapping with high-frequency ES is regarded as one of the gold standard methods for mapping language areas during awake craniotomy, but it may induce seizures. In the present pilot study, the fMRI shiritori word

generation task located the AL (100%) and PL in all but two patients (66%). When we could adopt other language tasks, such as reading or listening, that activates the PL in a more efficient way by using fMRI or magnetoencephalography [Kamada et al., 2007; Saur et al., 2008], the CCEP connectivity pattern, together with preoperative tractography and functional mapping, could probe the interconnected AL and PL without high-frequency ES in individual patients. It should be noted that a wide craniotomy was needed for intraoperative language network monitoring in order to place subdural electrodes to the perisylvian language areas as is the case with subcortical or cortical high frequency ES studies to identify language function [Berger et al., 1989; Kamada et al., 2007; Maldonado et al., 2011].

After defining the frontal stimulus site with the CCEP connectivity pattern, the integrity of the dorsal language pathway was monitored online by stimulating the AL and recording CCEPs from the temporoparietal area in a sequential manner. Online sequential CCEP monitoring was feasible during awake craniotomy, because of the high reproducibility and reliability of CCEP waveforms (amplitude, latency). Moreover, intraoperative CCEP monitoring was performed safely, without provoking any adverse events such as seizures during surgical procedures in all patients. A decrease of CCEP amplitude by less than 32% did not produce persistent language impairment in our case series. However, our pilot study could not yield a clear cut-off value due to a limited number of participants. By analogy to MEP [Macdonald, 2006], 50% might be an appropriate cut-off value, but further case accumulation is warranted for establishing the sensitivity and specificity of this method for its clinical usefulness.

In Patient 2, brain edema surrounding the tumor was too extensive to trace the AF tract into the posterior temporal area, even by probabilistic diffusion tractography. Despite brain edema, CCEP was recorded from the STG and MTG where the PL was indicated by the fMRI shiritori word generation task. The discrepancy in the positive rate between the fMRI language task and tractography is well documented in patients with brain tumors. Bizzi et al. [2012] reported that in 19 patients with glioma in the ventrolateral frontal region, the IFGop was identified with fMRI (verb generation task) in 17 patients (95%), while the AF was detected only in five patients (26%), dislocated in eight patients, and interrupted in six patients. In Patient 2, although the CCEP amplitude decreased by 12%, language function was preserved during and after surgery. The integrity of the subcortical language pathway could be monitored intraoperatively by CCEPs even when diffusion tractography failed to trace the AF tract beyond the region of brain edema.

Because of possible brain shift during awake craniotomy, the exact relationship between the site of subcortical ES and the AF was evaluated by postoperative MRI. The stimulus sites corresponded with the AF in three of five patients (60%). The concordance rate was similar to the one reported in a previous study combining subcortical high-frequency ES and diffusion tensor tractography [Ellmore et al., 2009]. The disconcordance usually resulted in negative findings as in Patient 1. Alternatively, stimulation of other language-related tracts [Ellmore et al., 2009] or that of the sulcal part of the cortex at the floor of removal cavity might lead to false positive findings, e.g., language impairment or SCEP responses whose latencies did not fit $CCEP_{AL \rightarrow PL}$ latency as in Patient 6. Combined 50 Hz and single-pulse subcortical ES would complement diffusion tractography and help clarify the site of stimulation for intraoperative language mapping.

Kokkinos et al. [2013] reported that delayed responses evoked by single-pulse ES showed similar topography between general anesthesia and awake condition. In the present study, although the amplitudes were less than those recorded in the awake condition, CCEPs were well recorded under general anesthesia and the CCEP connectivity pattern could localize the AL and PL in all patients. In patients in whom electrode location did not change throughout surgery, the CCEP distribution did not change (i.e., did not get larger) in the awake condition. When combined with noninvasive functional and anatomical neuroimaging techniques, intraoperative language network mapping under general anesthesia would be promising for preservation of the dorsal language network. Comparing the findings under general anesthesia with those during the awake condition in a larger number of patients is warranted to establish its clinical utility. Moreover, a similar intraoperative network mapping would be applicable for the ventral language pathway involved in language comprehension. The target white matter pathways for this network would be either the inferior longitudinal fasciculus or the inferior frontooccipital fasciculus, since 50 Hz white matter ES elicited semantic paraphasia [Duffau et al., 2005; Mandonnet et al., 2007]. To this end, combined 50 Hz and single-pulse ES should be applied first during awake craniotomy to probe the cortical and white matter function and their connections.

ACKNOWLEDGMENT

Authors are indebted to Dr. Masato Hojo for providing the patients' data.

REFERENCES

Behrens TE, Berg HJ, Jbabdi S, Rushworth MF, Woolrich MW (2007): Probabilistic diffusion tractography with multiple fibre orientations: What can we gain? NeuroImage 34:144–155.

Berger MS, Kincaid J, Ojemann GA, Lettich E (1989): Brain mapping techniques to maximize resection, safety, and seizure control in children with brain tumors. Neurosurgery 25:786–792.

Bizzi A, Nava S, Ferré F, Castelli G, Aquino D, Ciaraffa F, Broggi G, DiMeco F, Piacentini S (2012): Aphasia induced by gliomas growing in the ventrolateral frontal region: Assessment with diffusion MR tractography, functional MR imaging and neuropsychology. Cortex 48:255–272.

Catani M, Dell'acqua F, Bizzi A, Forkel SJ, Williams SC, Simmons A, Murphy DG, Thiebaut de Schotten M (2012): Beyond cortical localization in clinico-anatomical correlation. Cortex 48: 1262–1287.

Catenoix H, Magnin M, Guénot M, Isnard J, Mauguiére F, Ryvlin P (2005): Hippocampal-orbitofrontal connectivity in human: An electrical stimulation study. Clin Neurophysiol 116:1779–1784.

Catenoix H, Magnin M, Mauguiére F, Ryvlin P (2011): Evoked potential study of hippocampal efferent projections in the human brain. Clin Neurophysiol 122:2488–2497.

Conner CR, Ellmore TM, DiSano MA, Pieters TA, Potter AW, Tandon N (2011): Anatomic and electro-physiologic connectivity of the language system: A combined DTI-CCEP study. Comput Biol Med 41:1100–1109.

Duffau H (2008): The anatomo-functional connectivity of language revisited. New insights provided by electrostimulation and tractography. Neuropsychologia 46:927–934.

Duffau H, Gatignol P, Mandonnet E, Peruzzi P, Tzourio-Mazoyer N, Capelle L (2005): New insights into the anatomo-functional connectivity of the semantic system: A study using cortico-subcortical electrostimulations. Brain 128:797–810.

Ellmore TM, Beauchamp MS, O'Neill TJ, Dreyer S, Tandon N (2009): Relationships between essential cortical language sites and subcortical pathways. J Neurosurg 111:755–766.

Enatsu R, Matsumoto R, Piao Z, O'Connor T, Horning K, Burgess RC, Bulacio J, Bingaman W, Nair DR (2013): Cortical negative motor network in comparison with sensorimotor network: A cortico-cortical evoked potential study. Cortex 49:2080–2096.

Felleman DJ, Van Essen DC (1991): Distributed hierarchical processing in the primate cerebral cortex. Cereb Cortex 1:1–47.

Glasser MF, Rilling JK (2008): DTI tractography of the human brain's language pathways. Cereb Cortex 18:2471–2482.

Hickok G, Poeppel D (2004): Dorsal and ventral streams: A framework for understanding aspects of the functional anatomy of language. Cognition 92:67–99.

Howard MA, Volkov IO, Mirsky R, Garell PC, Noh MD, Granner M, Damasio H, Steinschneider M, Reale RA, Hind JE, Brugge JF (2000): Auditory cortex on the human posterior superior temporal gyrus. J Comp Neurol 416:79–92.

Inoue M, Ueno T, Morita K, Shoji Y, Matsuoka T, Fujiki R, Abe T, Uchimura N (2011): Brain activities on fMRI using the shiritori task in normal subjects. Kurume Med J 57:109–115.

July J, Manninen P, Lai J, Yao Z, Bernstein M (2009): The history of awake craniotomy for brain tumor and its spread into Asia. Surg Neurol 71:621–624; discussion 624–625.

Kamada K, Todo T, Masutani Y, Aoki S, Ino K, Morita A, Saito N (2007): Visualization of the frontotemporal language fibers by tractography combined with functional magnetic resonance imaging and magnetoencephalography. J Neurosurg 106:90–98.

Keller CJ, Bickel S, Entz L, Ulbert I, Milham MP, Kelly C, Mehta AD (2011): Intrinsic functional architecture predicts electrically evoked responses in the human brain. Proc Natl Acad Sci USA 108:10308–10313.

Kokkinos V, Alarcón G, Selway RP, Valentín A (2013): Role of single pulse electrical stimulation (SPES) to guide electrode implantation under general anaesthesia in presurgical assessment of epilepsy. Seizure 22:198–204.

Koubeissi MZ, Lesser RP, Sinai A, Gaillard WD, Franaszczuk PJ, Crone NE (2012): Connectivity between perisylvian and bilateral basal temporal cortices. Cereb Cortex 22:918–925.

Kubota Y, Enatsu R, Gonzalez-Martinez J, Bulacio J, Mosher J, Burgess RC, Nair DR (2013): *In vivo* human hippocampal cingulate connectivity: A corticocortical evoked potentials (CCEPs) study. Clin Neurophysiol 124:1547–1556.

Lacruz ME, García Seoane JJ, Valentin A, Selway R, Alarcón G (2007): Frontal and temporal functional connections of the living human brain. Eur J Neurosci 26:1357–1370.

Leclercq D, Duffau H, Delmaire C, Capelle L, Gatignol P, Ducros M, Chiras J, Lehéricy S (2010): Comparison of diffusion tensor imaging tractography of language tracts and intraoperative subcortical stimulations. J Neurosurg 112:503–511.

Macdonald DB (2006): Intraoperative motor evoked potential monitoring: overview and update. J Clin Monit Comput 20: 347–377.

Maldonado IL, Moritz-Gasser S, Duffau H (2011): Does the left superior longitudinal fascicle subserve language semantics? A brain electrostimulation study. Brain Struct Funct 216:263–274.

Mandonnet E, Nouet A, Gatignol P, Capelle L, Duffau H (2007): Does the left inferior longitudinal fasciculus play a role in language? A brain stimulation study. Brain 130:623–629.

Martino J, De Witt Hamer PC, Berger MS, Lawton MT, Arnold CM, de Lucas EM, Duffau H (2013): Analysis of the subcomponents and cortical terminations of the perisylvian superior longitudinal fasciculus: A fiber dissection and DTI tractography study. Brain Struct Funct 218:105–121.

Matsumoto R, Nair DR, LaPresto E, Najm I, Bingaman W, Shibasaki H, Lüders HO (2004): Functional connectivity in the human language system: A cortico-cortical evoked potential study. Brain 127:2316–2330.

Matsumoto R, Kinoshita M, Taki J, Hitomi T, Mikuni N, Shibasaki H, Fukuyama H, Hashimoto N, Ikeda A (2005): In vivo epileptogenicity of focal cortical dysplasia: A direct cortical paired stimulation study. Epilepsia 46:1744–1749.

Matsumoto R, Nair DR, LaPresto E, Bingaman W, Shibasaki H, Lüders HO (2007): Functional connectivity in human cortical motor system: A cortico-cortical evoked potential study. Brain 130:181–197.

Matsumoto R, Okada T, Mikuni N, Mitsueda-Ono T, Taki J, Sawamoto N, Hanakawa T, Miki Y, Hashimoto N, Fukuyama H, Takahashi R, Ikeda A (2008): Hemispheric asymmetry of the arcuate fasciculus. J Neurol 255:1703–1711.

Matsumoto R, Imamura H, Inouchi M, Nakagawa T, Yokoyama Y, Matsuhashi M, Mikuni N, Miyamoto S, Fukuyama H, Takahashi R, Ikeda A (2011): Left anterior temporal cortex actively engages in speech perception: A direct cortical stimulation study. Neuropsychologia 49:1350–1354.

Matsumoto R, Nair DR, Ikeda A, Fumuro T, Lapresto E, Mikuni N, Bingaman W, Miyamoto S, Fukuyama H, Takahashi R, Najm I, Shibasaki H, Lüders HO (2012): Parieto-frontal network in humans studied by cortico-cortical evoked potential. Hum Brain Mapp 33:2856–2872.

Matsuzaki N, Juhász C, Asano E (2013): Cortico-cortical evoked potentials and stimulation-elicited gamma activity preferentially propagate from lower- to higher-order visual areas. Clin Neurophysiol 124:1290–1296.

Mori S, van Zijl PC (2002): Fiber tracking: Principles and strategies—A technical review. NMR Biomed 15:468–480.

Oguri T, Sawamoto N, Tabu H, Urayama S, Matsuhashi M, Matsukawa N, Ojika K, Fukuyama H (2013): Overlapping connections within the motor cortico-basal ganglia circuit: fMRI-tractography analysis. NeuroImage 78:353–362.

Rosenberg DS, Mauguiére F, Catenoix H, Faillenot I, Magnin M (2009): Reciprocal thalamocortical connectivity of the medial pulvinar: A depth stimulation and evoked potential study in human brain. Cereb Cortex 19:1462–1473.

Saur D, Kreher BW, Schnell S, Kummerer D, Kellmeyer P, Vry MS, Umarova R, Musso M, Glauche V, Abel S, Huber W, Rijntjes M, Hennig J, Weiller C (2008): Ventral and dorsal pathways for language. Proc Natl Acad Sci USA 105:18035–18040.

Silbergeld DL, Mueller WM, Colley PS, Ojemann GA, Lettich E (1992): Use of propofol (Diprivan) for awake craniotomies: Technical note. Surg Neurol 38:271–272.

Smith SM, Jenkinson M, Woolrich MW, Beckmann CF, Behrens TE, Johansen-Berg H, Bannister PR, De Luca M, Drobnjak I, Flitney DE, Niazy RK, Saunders J, Vickers J, Zhang Y, De Stefano N, Brady JM, Matthews PM (2004): Advances in functional and structural MR image analysis and implementation as FSL. NeuroImage 23 (Suppl. 1):S208–S219.

Takayama M, Miyamoto S, Ikeda A, Mikuni N, Takahashi JB, Usui K, Satow T, Yamamoto J, Matsuhashi M, Matsumoto R, Nagamine T, Shibasaki H, Hashimoto N (2004): Intracarotid propofol test for speech and memory dominance in man. Neurology 63:510–515.

Terada K, Umeoka S, Usui N, Baba K, Usui K, Fujitani S, Matsuda K, Tottori T, Nakamura F, Inoue Y (2012): Uneven interhemispheric connections between left and right primary sensorimotor areas. Hum Brain Mapp 33:14–26.

Wakana S, Caprihan A, Panzenboeck MM, Fallon JH, Perry M, Gollub RL, Hua K, Zhang J, Jiang H, Dubey P, Blitz A, van Zijl P, Mori S (2007): Reproducibility of quantitative tractography methods applied to cerebral white matter. NeuroImage 36: 630–644.

Whitaker HA, Ojemann GA (1977): Graded localisation of naming from electrical stimulation mapping of left cerebral cortex. Nature 270:50–1.

Yogarajah M, Focke NK, Bonelli SB, Thompson P, Vollmar C, McEvoy AW, Alexander DC, Symms MR, Koepp MJ, Duncan JS (2010): The structural plasticity of white matter networks following anterior temporal lobe resection. Brain 133:2348–2364.

Acta Radiologica
2015, Vol. 56(1) 114–120

DOI: 10.1177/0284185114521187
acr.sagepub.com
SAGE

Estimation of proliferative potentiality of central neurocytoma: correlational analysis of minimum ADC and maximum SUV with MIB-1 labeling index

Ryo Sakamoto[1], Tomohisa Okada[1], Mitsunori Kanagaki[1], Akira Yamamoto[1], Yasutaka Fushimi[1], Takahide Kakigi[1], Yoshiki Arakawa[2], Jun C Takahashi[2], Yoshiki Mikami[3] and Kaori Togashi[1]

Abstract

Background: Central neurocytoma was initially believed to be benign tumor type, although atypical cases with more aggressive behavior have been reported. Preoperative estimation for proliferating activity of central neurocytoma is one of the most important considerations for determining tumor management.

Purpose: To investigate predictive values of image characteristics and quantitative measurements of minimum apparent diffusion coefficient (ADCmin) and maximum standardized uptake value (SUVmax) for proliferative activity of central neurocytoma measured by MIB-1 labeling index (LI).

Material and Methods: Twelve cases of central neurocytoma including one recurrence from January 2001 to December 2011 were included. Preoperative scans were conducted in 11, nine, and five patients for computed tomography (CT), diffusion-weighted imaging (DWI), and fluorine-18-fluorodeoxyglucose positron emission tomography (FDG-PET), respectively, and ADCmin and SUVmax of the tumors were measured. Image characteristics were investigated using CT, T2-weighted (T2W) imaging and contrast-enhanced T1-weighted (T1W) imaging, and their differences were examined using the Fisher's exact test between cases with MIB-1 LI below and above 2%, which is recognized as typical and atypical central neurocytoma, respectively. Correlational analysis was conducted for ADCmin and SUVmax with MIB-1 LI. A P value <0.05 was considered significant.

Results: Morphological appearances had large variety, and there was no significant correlation with MIB-1 LI except a tendency that strong enhancement was observed in central neurocytomas with higher MIB-1 LI ($P = 0.061$). High linearity with MIB-1 LI was observed in ADCmin and SUVmax ($r = -0.91$ and 0.74, respectively), but only ADCmin was statistically significant ($P = 0.0006$).

Conclusion: Central neurocytoma had a wide variety of image appearance, and assessment of proliferative potential was considered difficult only by morphological aspects. ADCmin was recognized as a potential marker for differentiation of atypical central neurocytomas from the typical ones.

Keywords

Central neurocytoma, central nervous system (CNS), brain, MR diffusion, positron emission tomography (PET)

Date received: 12 November 2013; accepted: 6 January 2014

[1]Department of Diagnostic Imaging and Nuclear Medicine, Kyoto University Graduate School of Medicine, Kyoto, Japan
[2]Department of Neurosurgery, Kyoto University Graduate School of Medicine, Kyoto, Japan
[3]Department of Clinical Pathology, Kyoto University Graduate School of Medicine, Kyoto, Japan

Corresponding author:
Tomohisa Okada, Department of Diagnostic Imaging and Nuclear Medicine, Kyoto University Graduate School of Medicine, 54 Shogoin Kawahara-cho, Sakyo-ku, Kyoto, 606-8507, Japan.
Email: tomokada@kuhp.kyoto-u.ac.jp

Introduction

Central neurocytoma is a rare low grade tumor of the central nervous system, which was first described by Hassoun et al. in 1982 (1). It is composed of uniform

round cells with neuronal differentiation constituting approximately 0.25–0.5% of all intracranial tumors. It occurs typically in young adults and is located in the lateral or third ventricle around the foramen of Monro (2). The clinical course of central neurocytomas was initially believed to be benign, however, more aggressive behavior including rapid tumor progression, recurrence, extra-ventricular extension, and craniospinal dissemination has been described (3,4). The term atypical central neurocytoma has been proposed for an aggressive variant, which is classified if MIB-1 (Immunotech, Marseilles, France) labeling index (LI), an index of cellular proliferation, is higher than 2% (5) or atypical histologic features of focal necrosis, vascular proliferation, and increased mitotic activity are observed (6). MIB-1 is a monoclonal antibody to Ki-67 antigen that is a nuclear protein associated with cellular proliferation.

For patients with an atypical central neurocytoma, complete resection is the best treatment for better local control and survival (7). Therefore, preoperative estimation for proliferating activity of a central neurocytoma is one of the most important considerations for determining the appropriate surgical strategy. There are some reports discussing imaging features of the central neurocytoma. They reported varying degrees of contrast enhancement with or without cystic appearance and calcification of tumors (8,9), but focused mainly on differentiating neurocytomas from other intraventricular tumors. The relationship between proliferative potential and morphological imaging findings has not been clarified.

As quantitative imaging marker of malignancy, diffusion-weighted imaging (DWI) provides further physiologic information as apparent diffusion coefficient (ADC), which is helpful in grading brain tumors (10,11) including central neurocytoma (12). ADC correlates with tumor cellularity, prognosis, and MIB-1 LI in gliomas (13–15). Standardized uptake value (SUV) measured by 18F-fluorodeoxyglucose-positron emission tomography (FDG-PET) reflects increased glucose metabolism and correlates with histological grade of gliomas (16). Mineura et al. reported rapid regrowth of central neurocytoma that increased the cerebral metabolic rate of glucose (17). Ohtani et al. reported a case of central neurocytoma with intense FDG uptake, which had a high MIB-1 LI and atypical pathological features (18). These cases indicate that SUV may also predict the proliferation potential of central neurocytomas. However, preoperative estimation of the proliferative activity of the central neurocytoma has not been conducted.

Therefore in this study, we investigated if image characteristics and quantitative values of ADC and SUV could distinguish central neurocytomas with MIB-1 LI higher than 2% from those with lower values.

Material and Methods

This study was approved by institutional review board, and informed consent was waived, because retrospective analysis was conducted.

Patients

Eleven patients from January 2001 to December 2011 at our institute were enrolled. Inclusion criteria was pathological confirmation of central neurocytoma and presence of preoperative imaging studies (computed tomography [CT], magnetic resonance imaging [MRI], and FDG-PET). There was one recurrent case at 3 years after partial tumor resection (patient 4 in Table 1). This case was enrolled as patient 4', and images just before the secondary operation were also analyzed.

CT imaging

CT images were obtained parallel to the orbitomeatal line. Resolutions of all CT images were $0.4 \times 0.4 \times 7$–8 mm.

MRI

MR scans were conducted with 1.5 T scanners for six patients (patients 1, 3, 4, 4', and 6 with MAGNETOM Symphony, Siemens Medical Systems, Erlangen, Germany; patients 2 and 5 with Signa Genesis, GE Healthcare, Milwaukee, WI, USA) and 3 T scanners for five patients (patients 7, 8, and 9 with MAGNETOM Trio; patients 10 and 11 with MAGNETOM Skyra, Siemens Medical Systems, Erlangen, Germany). In addition to conventional axial T1-weighted (T1W) imaging (TR/TE, 450–616/8.1–12 ms) and T2-weighted (T2W) imaging (TR/TE, 3180–7960/93–130 ms), contrast-enhanced axial T1W images were acquired after administration of the gadolinium contrast agent (0.1 mmol/kg) in 11 cases. DWI was acquired in nine cases with in-plane resolution = 0.69–1.38 mm and slice thickness/spacing = 3–5/1–1.5 mm using a single-shot echo-planar sequence with motion-probing gradients ($b = 0$, 1000 s/mm^2) applied in three orthogonal directions, and ADC map was calculated.

PET imaging

FDG-PET scans were conducted using a PET scanner for one patient and a PET/CT scanner for four patients

Table 1. Characteristics of the patients and tumor images.

Patient no.	Sex/Age (years)	Location	Size (mm)	Calcification on CT distribution/density	Cystic appearance on T2WI distribution/ uniformity/size	Enhancement on Gd-T1W imaging degree/ homogeneity
1	M/31	LtLV~3V	54 × 43	Diffuse/dense	Diffuse/non-uniform/large	None/n.a.
2	F/34	RtLV	61 × 39	Patchy/dense	Diffuse/non-uniform/large	n.a./n.a.
3	M/35	RtLV	39 × 18	None	Diffuse/uniform/small	None/n.a.
4	F/21	RtLV	42 × 37	Patchy/faint	Partial/non-uniform/small	Marked/heterogeneous
4'	F/24	RtLV	27 × 20	None	Partial/uniform/small	Marked/homogeneous
5	F/38	LtLV	39 × 25	Patchy/dense	Diffuse/non-uniform/large	Slight/homogeneous
6	F/54	LtLV	63 × 44	None	Partial/non-uniform/large	Marked/homogeneous
7	M/22	LtLV~3V	59 × 40	Patchy/faint	Diffuse/non-uniform/small	None/n.a.
8	M/28	LtLV	27 × 19	None	Partial/uniform/small	Moderate/heterogeneous
9	M/34	RtLV	29 × 25	Patchy/faint	Diffuse/non-uniform/large	None/n.a.
10	M/34	LtLV	21 × 17	None	Diffuse/uniform/small	Moderate/homogeneous
11	M/26	LtLV	15 × 13	None	Partial/uniform/small	None/n.a.

3V, third ventricle; Gd-T1WI, gadolinium-enhanced T1-weighted imaging; LtLV, left lateral ventricle; n.a., not applicable; RtLV, right lateral ventricle; T2WI, T2-weighted imaging.

(patient 4′ with Advance; patients 8 to 11 with Discovery ST Elite, GE Healthcare, Waukesha, WI, USA). Patients fasted for at least 4 h prior to the scans. After intravenous administration of 4 MBq/kg of FDG, patients rested in a waiting room for 30 min. Emission scans of the brain were conducted for 15 min. Resolutions were 2.0 × 2.0 × 4.25 mm (35 slices) and 2.0 × 2.0 × 3.27 mm (47 slices), respectively, for the scanners.

Image analysis

Appearance of the tumors was reviewed with regard to location, size, calcification on CT image (present/absent: if present, distribution = diffuse or patchy; density = faint or dense), cystic components on T2W imaging (distribution = diffuse or partial; uniformity = uniform or non-uniform; size = small or large), and degree of enhancement on contrast-enhanced T1W imaging (degree = none to slight or moderate to marked; homogeneity = homogeneous or heterogeneous), and categorized by two board-certified neuroradiologists in consensus (RS and TK, both with experience in diagnostic imaging for 8 years).

For quantitative analysis, regions of interest (ROIs) were defined independently by two neuroradiologists (RS and TK) at different areas (2 to 3 areas) within the tumors of the ADC maps and SUV images (ROI size, 50–361 mm^2 and 114–513 mm^2, respectively) using free software (MRIcro, http://www.mccauslandcenter.sc.edu/mricro/, provided by Chris Rorden, Neuropsychology Lab, Columbia SC, USA). Care was taken to exclude macroscopic calcifications and cysts on each modality referencing to CT image and T2W imaging. From the values of the ROIs, minimum ADC (ADCmin) and maximum SUV (SUVmax) were extracted.

Proliferative activity

Proliferative activity was measured as MIB-1 LI in formalin-fixed paraffin embedded pathological specimens with immuno-histochemical staining using MIB-1 monoclonal antibody. Areas with highest number of positive nuclei were identified, and a minimum of 1000 cells were counted in each tissue section (by YM, a board-certified pathologist majoring in surgical neuropathology). MIB-1 LI was defined as the percentage of tumor cells which stained positively for Ki-67 nuclear antigen.

Statistical analysis

Intra-class correlation coefficients (ICCs) for measured values in the ROIs were evaluated. Image characteristics were compared between two tumor groups with MIB-1 LI lower to equal to or higher than 2% using Fisher's exact test. ADCmin and SUVmax values were assessed by linear regression analyses with values of MIB-1 LI. ROC analysis was conducted to investigate differential capability of atypical central neurocytomas from typical ones, when there was a significant correlation. A P value <0.05 was considered statistically significant. Statistical analyses were conducted using

commercially available software (MedCalc, version 12.4.0; MedCalc Software, Acacialaan 22, B-8400 Ostend, Belgium).

Results

Characteristics of the patients and tumor images are summarized in Table 1. All of the tumors were located in the lateral ventricle and had an attachment to the ventricular wall or septum pellucidum. CT scans showed calcifications of variable density and distribution. Almost all tumors had heterogeneous appearance with solid portions and cysts that were variable in number and size. MRI showed that most tumors were iso- to hypo-intense on T1W imaging and hyper-intense on T2W imaging. Contrast enhancement of tumors was homogenous or heterogeneous, and degree of enhancement varied. Six tumors showed none to slight enhancement and five tumors had moderate to marked enhancement. It was a tendency that strong enhancement was observed in tumors with higher MIB-1 LI ($P = 0.061$). There was no significant difference in other image characteristics. Fig. 1 shows representative case images (patient 10) and Fig. 2 visually summarizes image characteristics.

The quantitative values of MIB-1 LI, ADCmin, and SUVmax are listed in Table 2. Fig. 3 shows DWI, ADC map, and FDG-PET/CT images of a representative case. MIB-1 LI was in the range of 0.09–5.62% (mean $\pm$ SD, $3.26 \pm 1.88\%$). Four tumors had MIB-1 LI lower than 2%, and eight tumors had those higher than 2%. ICCs of the ROI analyses were 0.97 for ADCmin and 0.96 for SUVmax, which means excellent agreements. ADCmin values ranged from 0.23 to $1.05 \times 10^{-3}\,mm^2/s$, and significant linear correlation

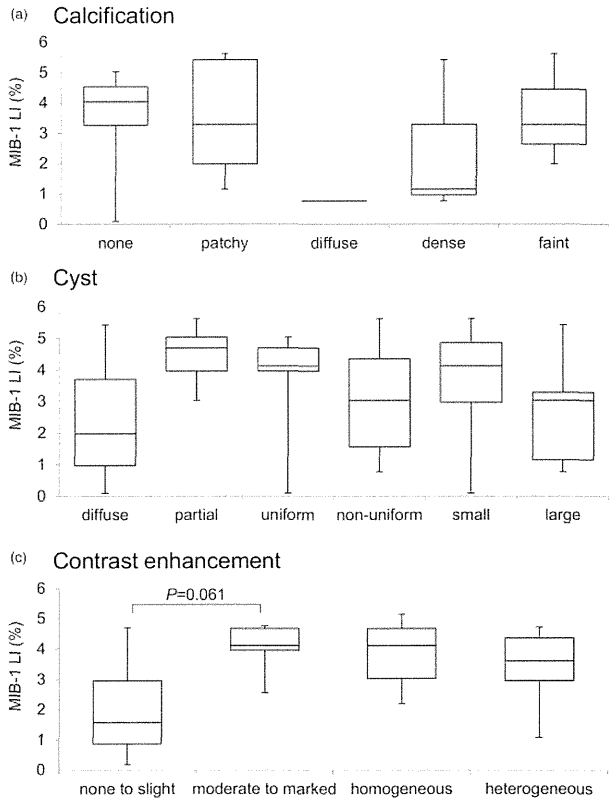

Fig. 2. Box plots show the relationship of MIB-1 LI values with the following image characteristics: (a) calcification on CT (none or present, patchy or diffuse, and dense or faint), (b) cysts on T2W imaging (diffuse or partial, uniform or non-uniform, and small or large), and (c) contrast enhancement on T1W imaging (none to slight or moderate to marked, and homogeneous or heterogeneous). Image characteristics of tumors varies greatly and only the difference in contrast enhancement between none to slight and moderate to marked is marginally significant ($P = 0.061$) between tumors with MIB-1 LI lower or higher than 2% using Fisher's exact test.

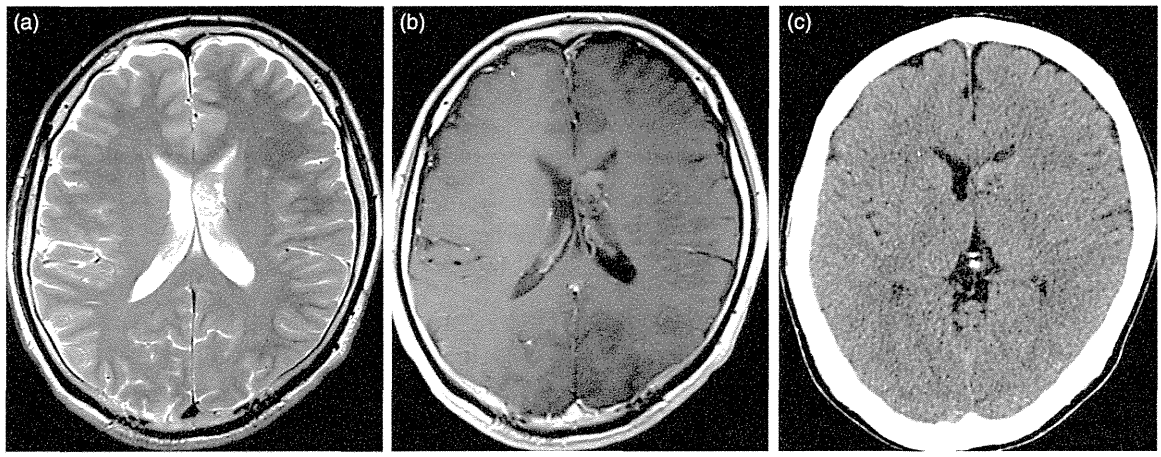

Fig. 1. A representative case of a central neurocytoma located at the left lateral ventricle (patient 10). Diffusely distributed small cysts on T2W imaging (a) and moderately enhanced solid portion on contrast-enhanced T1W imaging (b) are noted. Calcification is not identified on CT (c).

Table 2. MIB-1 LI, ADCmin, and SUVmax of the central neurocytomas.

Patient no.	MIB-1 LI (%)	ADCmin (10^{-3} mm^2/s)	SUVmax
1	0.77	0.92	n.a.
2	5.42	n.a.	n.a.
3	0.09	0.95	n.a.
4	5.62	0.45	n.a.
4'	4.68	n.a.	7.61
5	1.15	1.05	n.a.
6	3.03	n.a.	n.a.
7	1.98	0.73	n.a.
8	3.95	0.45	5.60
9	3.28	0.55	3.35
10	4.12	0.26	4.55
11	5.03	0.23	5.61

ADCmin, minimum value of ADC in the tumor ROI; MIB-1 LI, MIB-1 labeling index; n.a., not applicable; SUVmax, maximum of SUV.

was observed with MIB-1 LI ($r = -0.91$, $P = 0.0006$). ROC analysis showed that atypical central neurocytomas could be differentiated from typical ones with 100% sensitivity (95% CI, 47.8–100.0%) and 100% specificity (39.8–100.0%), when the threshold value of ADCmin was set at 0.55×10^{-3} mm^2/s ($P < 0.0001$). The SUVmax was in the range of 3.35–7.61. The values had high correlation with MIB-1 LI ($r = 0.74$), but it was not significant ($P = 0.15$). These linear relationships are presented in Fig. 4.

Discussion

Although central neurocytomas have been considered indolent, there are some cases with aggressive biologic behavior including postoperative rapid regrowth (19,20). Among many pathologic features, elevated MIB-1 LI correlates with an increased recurrence rate and poor outcome (5,21) and is thought to be a reliable

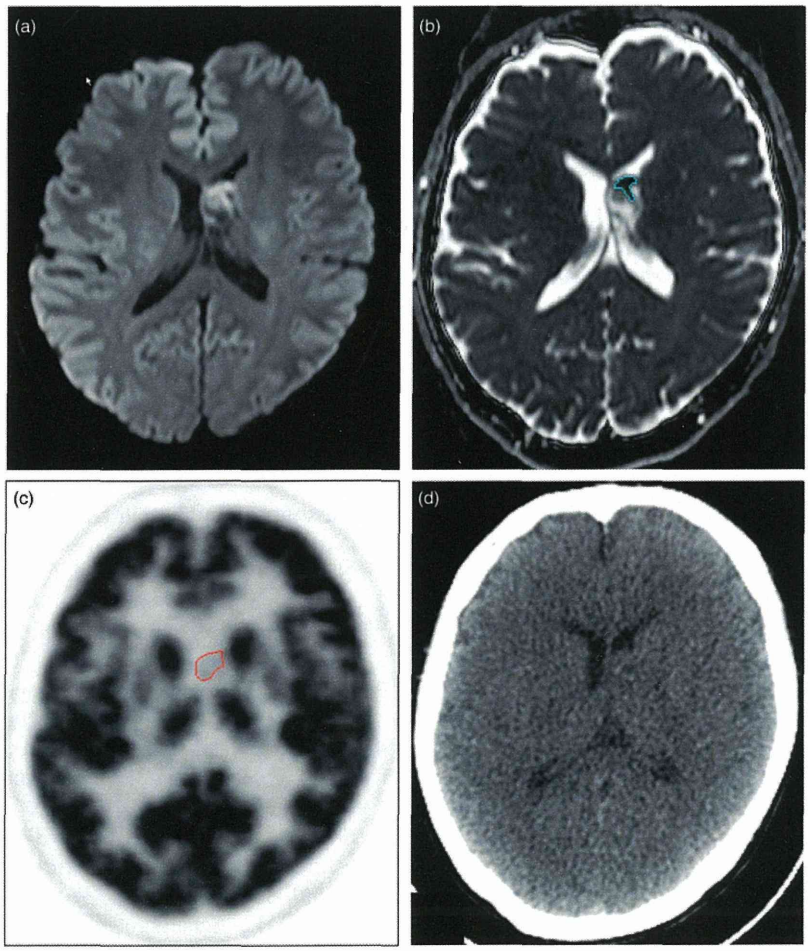

Fig. 3. The solid portion of the tumor in the representative case shows high signal on DWI (a) and restricted diffusion on ADC map, where a ROI for ADCmin is drawn (b). A ROI for SUVmax is defined at the same location on FDG-PET (c), referring to simultaneously acquired CT image (d).

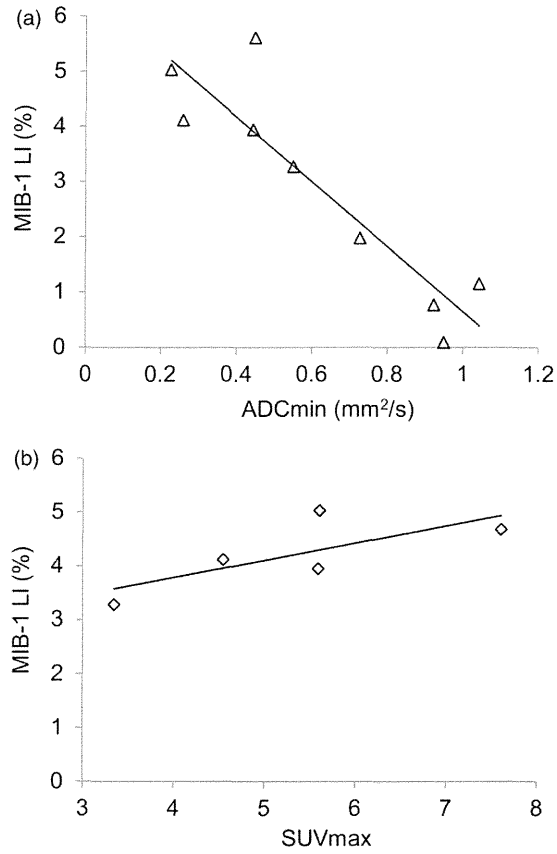

Fig. 4. (a) Linear regression analyses shows significant negative correlation ($r = -0.9$) between ADCmin and MIB-1 LI ($P = 0.0006$). (b) There is high correlation between SUVmax and MIB-1 LI ($r = 0.74$), but it is not statistically significant ($P = 0.15$).

immune-histopathologic marker (5). No significant correlation was found between other histopathologic characteristics and clinical outcome (22,23). In this study, a large variety was observed in calcification and cystic changes, and only strong enhancement suggested increased proliferative potential as in the former case reports (24,25).

Our result of MIB-1 LI is congruent with the previous reports ranging from less than 0.1 to 11.2% (5,21,23). There was a significant negative linear correlation between MIB-1 LI and ADCmin as in other types of brain tumors (13). ADC values have an inverse relationship with tumor grades (10,26), and poor survival has been reported in malignant glial tumors with lower ADCmin (14,27). Our result indicates that lower ADCmin reflects malignant potential of central neurocytomas. In the case of patient 4, the tumor had a high MIB-1 LI (5.62%) with a lower ADCmin ($0.45 \times 10^{-3}\,mm^2/s$) than the proposed threshold. After partial resection, the tumor regrew gradually in the 3-year follow-up (patient 4'). The recurrent tumor showed a high SUVmax (7.61) before a second operation, and the pathologic specimen revealed that tumor maintained high proliferative activity (MIB-1 LI = 4.68%).

Increased glucose metabolism indicates higher proliferative activity of the brain tumor (28). Our study presented high linearity between SUVmax and MIB-1 LI. This result may help to facilitate the usage of FDG-PET examinations in central neurocytomas as in a previous case report, which demonstrated that a central neurocytoma with higher FDG uptake showed an increased proliferative index associated with atypical histological features (18).

There are several limitations in this study. First, the number of cases is small. However, it is considered inevitable, because the central neurocytoma is relatively rare. Because of this rarity, the enrollment period was very long. Therefore not all image examinations were available, and different scanners and parameters were used, particularly in MRI.

In conclusion, central neurocytomas have a variety of image appearances, with no significant correlation with MIB-1 LI except a tendency that central neurocytomas with higher MIB-1 LI demonstrated stronger enhancement. Assessment of proliferative potential would be difficult if only morphological aspects are considered. ADCmin showed significant linear correlation with MIB-1 LI, and SUVmax had the same tendency. Both quantitative imaging values of ADCmin and SUVmax, especially for ADCmin, are considered as potential markers for predicting high MIB-1 LI of central neurocytoma.

Funding

This research received no specific grant from any funding agency in the public, commercial, or not-for-profit sectors.

References

1. Hassoun J, Gambarelli D, Grisoli F, et al. Central neurocytoma. An electron-microscopic study of two cases. Acta Neuropathol 1982;56:151–156.
2. Hassoun J, Soylemezoglu F, Gambarelli D, et al. Central neurocytoma: a synopsis of clinical and histological features. Brain Pathol 1993;3:297–306.
3. Bertalanffy A, Roessler K, Koperek O, et al. Recurrent central neurocytomas. Cancer 2005;104:135–142.
4. Takao H, Nakagawa K, Ohtomo K. Central neurocytoma with craniospinal dissemination. J Neurooncol 2003; 61:255–259.
5. Soylemezoglu F, Scheithauer BW, Esteve J, et al. Atypical central neurocytoma. J Neuropathol Exp Neurol 1997; 56:551–556.
6. Brat DJ, Scheithauer BW, Eberhart CG, et al. Extraventricular neurocytomas: pathologic features and clinical outcome. Am J Surg Pathol 2001;25:1252–1260.
7. Rades D, Fehlauer F, Schild SE. Treatment of atypical neurocytomas. Cancer 2004;100:814–817.

8. Zhang B, Luo B, Zhang Z, et al. Central neurocytoma: a clinicopathological and neuroradiological study. Neuroradiology 2004;46:888–895.
9. Chen H, Zhou R, Liu J, et al. Central neurocytoma. J Clin Neurosci 2012;19:849–853.
10. Kono K, Inoue Y, Nakayama K, et al. The role of diffusion-weighted imaging in patients with brain tumors. Am J Neuroradiol 2001;22:1081–1088.
11. Bulakbasi N, Guvenc I, Onguru O, et al. The added value of the apparent diffusion coefficient calculation to magnetic resonance imaging in the differentiation and grading of malignant brain tumors. J Comput Assist Tomogr 2004;28:735–746.
12. Kocaoglu M, Ors F, Bulakbasi N, et al. Central neurocytoma: proton MR spectroscopy and diffusion weighted MR imaging findings. Magn Reson Imaging 2009; 27:434–440.
13. Higano S, Yun X, Kumabe T, et al. Malignant astrocytic tumors: clinical importance of apparent diffusion coefficient in prediction of grade and prognosis. Radiology 2006;241:839–846.
14. Zulfiqar M, Yousem DM, Lai H. ADC values and prognosis of malignant astrocytomas: does lower ADC predict a worse prognosis independent of grade of tumor?–a meta-analysis. Am J Roentgenol 2013;200:624–629.
15. Le Bihan D. Apparent diffusion coefficient and beyond: what diffusion MR imaging can tell us about tissue structure. Radiology 2013;268:318–322.
16. Padma MV, Said S, Jacobs M, et al. Prediction of pathology and survival by FDG PET in gliomas. J Neurooncol 2003;64:227–237.
17. Mineura K, Sasajima T, Itoh Y, et al. Blood flow and metabolism of central neurocytoma: a positron emission tomography study. Cancer 1995;76:1224–1232.
18. Ohtani T, Takahashi A, Honda F, et al. Central neurocytoma with unusually intense FDG uptake: case report. Ann Nucl Med 2001;15:161–165.
19. Warmuth-Metz M, Klein R, Sorensen N, et al. Central neurocytoma of the fourth ventricle. Case report. J Neurosurg 1999;91:506–509.
20. Wharton SB, Antoun NM, Macfarlane R, et al. The natural history of a recurrent central neurocytoma-like tumor. Clin Neuropathol 1998;17:136–140.
21. Mackenzie IR. Central neurocytoma: histologic atypia, proliferation potential, and clinical outcome. Cancer 1999;85:1606–1610.
22. Vasiljevic A, Francois P, Loundou A, et al. Prognostic factors in central neurocytomas: a multicenter study of 71 cases. Am J Surg Pathol 2012;36:220–227.
23. Ashkan K, Casey AT, D'Arrigo C, et al. Benign central neurocytoma. Cancer 2000;89:1111–1120.
24. Ogawa Y, Sugawara T, Seki H, et al. Central neurocytomas with MIB-1 labeling index over 10% showing rapid tumor growth and dissemination. J Neurooncol 2006; 79:211–216.
25. Kuchiki H, Kayama T, Sakurada K, et al. Two cases of atypical central neurocytomas. Brain Tumor Pathol 2002;19:105–110.
26. Lee EJ, Lee SK, Agid R, et al. Preoperative grading of presumptive low-grade astrocytomas on MR imaging: diagnostic value of minimum apparent diffusion coefficient. Am J Neuroradiol 2008;29:1872–1877.
27. Yamasaki F, Sugiyama K, Ohtaki M, et al. Glioblastoma treated with postoperative radio-chemotherapy: prognostic value of apparent diffusion coefficient at MR imaging. Eur J Radiol 2010;73:532–537.
28. Kruer MC, Kaplan AM, Etzl MM Jr. The value of positron emission tomography and proliferation index in predicting progression in low-grade astrocytomas of childhood. J Neurooncol 2009;95:239–245.